Case Studies in Thermal Engineering 34 (2022) 101937

Contents lists available at ScienceDirect

Case Studies in Thermal Engineering

journal homepage: www.elsevier.com/locate/csite

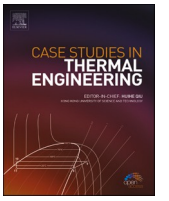

Effects of swirl enhancement on in-cylinder flow and mixture characteristics in a high-compression-ratio, spray-guided, gasoline direct injection engine

Jisoo Shin [a], Donghwan Kim [a], Yousang Son [b], Sungwook Park [c,*]

[a] Department of Mechanical Convergence Engineering, Graduate School of Hanyang University, Seoul, 04763, Republic of Korea
[b] Engine Advanced Development Team, Hyundai Motor Group, Republic of Korea
[c] School of Mechanical Engineering, Hanyang University, Seoul, 04763, Republic of Korea

ARTICLE INFO

Keywords:
High compression ratio
Gasoline direct injection
Spray-guided injection
Swirl control valve
Mixture formation

ABSTRACT

In this study, the flow enhancement effects of applying a swirl control valve were investigated with particle image velocimetry and simulation using CONVERGE v2.4 program in a high compression ratio, spray-guided, gasoline direct injection engine. This was followed by analysis of varying the spray structure and the mixture preparation process for different swirl control valve angles. The flow intensity was strengthened in the order of swirl control valve angle 45°, 30°, and 0°, and spark plug gap velocities near TDC were increased 1.89, 4.40, and 6.69 m/s in that order. However, the effect was not significant when it was increased to more than 45°. Also, the swirl-dominant flow and the tumble-dominant flow were differentiated based on the relationship between maximum swirl and tumble ratios. In the swirl dominant flow (swirl control valve angle of 0°), more retarded injection timing produced mixture formation in the order of homogenous to mal-distributed to stratified, whereas in the tumble dominant flow (swirl control valve angle of 45°), the order was homogenous to stratified to mal-distributed. It was determined by characteristic period to which the injection timing belonged, and the characteristic period was defined based on the relationship between the intake valve lift and the piston velocity.

Nomenclature

S/T	Ratio of maximum swirl ratio and maximum tumble ratio
V_d	Velocity difference between intake ports
$V_{port\ w/\ SCV}$	Velocity through the intake port with the swirl control valve
$V_{port\ w/o\ SCV}$	Velocity through the intake port without the swirl control valve
$\omega_{crank\ shaft}$	Angular velocity of crank shaft
$\omega_{swirl\ plane}$	Angular velocity of the flow about the center of mass in the swirl direction
$\omega_{tumble\ plane}$	Angular velocity of the flow about the center of mass in the tumble direction

ABBREVIATIONS

PEV	Pure electric vehicle

* Corresponding author. School of Mechanical Engineering, Hanyang University, 222 Wangsimni-ro, Seongdong-gu, Seoul, 04763, Republic of Korea.
E-mail address: parks@hanyang.ac.kr (S. Park).

https://doi.org/10.1016/j.csite.2022.101937
Received 20 December 2021; Received in revised form 23 February 2022; Accepted 11 March 2022
Available online 9 April 2022

ICE	Internal combustion engine
HCCI	Homogeneous charge compression ignition
GDI	Gasoline direct injection
SCV	Swirl control valve
PIV	Particle image velocimetry
CFD	Computational fluid dynamics
IVO	Intake valve open
IVC	Intake valve close
EVO	Exhaust valve open
EVC	Exhaust valve close
TDC	Top dead center
ER	Equivalence ratio

1. Introduction

With increasing concerns about environmental issues related to fossil fuel consumption and air pollution, more stringent regulations about emissions are being applied in the global transportation markets [1]. In response, the development of pure electric vehicles (PEVs) has grown in recent years. However, PEVs have certain challenges, including battery charging, driving range [2] and their energy storage systems [3]. Therefore, new combustion concepts for fuel economy and emission control in ICEs need to be developed, and many relevant studies are ongoing [4–7].

Homogeneous charge compression ignition (HCCI) combustion strategies have been proposed for achieving higher thermal efficiency and low NOx and particulate matter emissions [8]. HCCI combustion occurs with multi-point autonomous ignition under homogeneous charge mixture condition so that the combustion process is dominated by chemical kinetics. Since combustion takes place through spontaneous auto-ignition, it is applicable under very lean conditions, resulting in improved fuel economy [9]. Although the HCCI combustion concept has many advantages, it has limitations of a small operating range due to combustion noise and knocking combustion in high-load conditions [10], and controlling the ignition timing [11], which adversely affects the combustion stability. To address these issues, HCCI combustion control strategies consider fuel management [12], homogeneous charge preparation, and exhaust gas recirculation [13,14]. Also, a spark-assisted HCCI combustion concept helps to control ignition timing for handling the cycle-to-cycle variation of HCCI combustion [15]. Furthermore, Wang Z. et al. [16] found that with spark assist, not only the cycle-to-cycle variation but also the thermal efficiency improved compared to an HCCI engine without spark ignition.

With spark ignition, the combustion of a high compression ratio gasoline engine needs an appropriate charge mixture preparation (homogeneous or stratified). A gasoline direct injection (GDI) system has the advantage of producing the charge mixture characteristics demanded by the operating conditions, while securing higher volumetric efficiency than port fuel injection system. A GDI system in a wall-guided type, a spray-guided type or an air-guided type; most of them are the wall-guided, side-mount injection type [17]. However, in recent researches the spray-guided type of direct injection was adopted to incorporate a mixture stratification strategy [18] for lean conditions with late injection timing in spark assist high compression ratio gasoline engines. The spray-guided type has the potential to improve efficiency by emphasizing air flow and turbulence [19], and Zeng W. et al. [20] found that the flow intensified with spray-guided injection, which reduced the cyclic variation.

The in-cylinder tumble and swirl flows play an important role in stable combustion in GDI engines by affecting early flame propagation [21]. This is because the reinforced in-cylinder flow causes enhancement of the in-cylinder turbulent intensity [22] and flow in the vicinity of the spark plug, which is closely related to the ignition [23] followed by the combustion phase [24]. The knocking problem in the high compression ratio GDI engines [25], which causes cyclic variation, can be suppressed by forming sufficient turbulent intensity [26]. Therefore, suitable in-cylinder flow intensification strategies are required for high compression ratio GDI engines.

A swirl control valve (SCV) which is positioned in one of the intake ports can be adopted to manage the intake flow characteristics. The in-cylinder flow driven from the SCV affects not only the swirl flow but also the tumble flow. Furthermore, the spray characteristic is affected by the in-cylinder flow and the spray structure varies by the swirl ratio [27]. Along with considering the spray structure, it is necessary to understand the injection strategy based on the SCV angle because the mixture preparation is determined by the intensity of the swirl and tumble flow. Hosseini. et al. [28] have found that the elevating swirl intensity had advantage for combustion efficiency and NOx reduction because fuel and air mixed more efficiently.

Therefore, in this study, the SCV was considered as a method to improve the efficiency and combustion stability of a high compression ratio GDI engine, and the flow and spray characteristics for various SCV angles were analyzed with a two-cylinder high-compression ratio GDI engine. Depending on the SCV angle, the flow characteristics from the intake to near the spark timing vary, so the mixture preparations are affected. Thus, the characteristics of the intake port flow, in-cylinder flow, spray development, and the mixture near the spark timing was investigated sequentially using particle image velocimetry (PIV) experiment, Mie-scattering imaging, and CONVERGE v2.4 which is computational fluid dynamics (CFD) simulation program. The characteristic period was defined by correlating the flow development process over time with the intake valve movement and piston velocity. Additionally, the mixture properties were investigated according to which characteristic period the injection timing was included in. Based on the results, the effect of SCV angles on flow and mixture characteristics was analyzed.

2. Engine specification

In this study, a two-cylinder high compression ratio GDI engine was used for the experiments and simulations. The engine specifications are given in Table 1.

3. Experimental setup

In this study, the spray and in-cylinder flow were visualized by Mie-scattering and PIV imaging technique, respectively. The schematic diagrams of an optically accessible engine and PIV optical system are depicted in Fig. 1. A high-speed camera with a delay generator was used to visualize in both spray and in-cylinder flow visualization experiments. A Nd:YAG laser was used to form a 2-D laser sheet crossing the center of cylinder, and PIV images were captured at that plane. The cylinder to be visualized was selected as cylinder 2 in consideration of the photographing angle, and only the light source was replaced from Nd:YAG laser to metal-halide lamp for capturing the spray structure. Intake air was supplied through a mass flow meter and the intake pressure was maintained at 1.0 bar. A National Instruments CompactRIO real-time integrated controller was used to control the optically accessible engine. Fuel pump was used to realize the high injection pressure, and common rail was established to reduce the pressure fluctuation during fuel injection. The tracer was generated by seed generator. The tracer was inflowed into the intake air through the seed mixing chamber to control the flow rate and supply a uniform amount of tracer into the cylinder. The details of optically accessible system were drawn in Fig. 1(a). A laser sheet for capturing PIV images was generated by the planar convex and concave lenses, and it has thickness of 2 mm. The laser sheet was formed to pass through the center of the cylinder from intake valves to exhaust valves, as shown in Fig. 1(b). The tracer was selected as a hollow glass sphere with a diameter of 10 μm, and the region of interest was the entire cylinder except for a pent roof region due to design limitations. The captured PIV raw images were processed using a MATLAB (PIVlab, MathWorks, USA) [29]. The details about calculating tumble center and turbulent kinetic energy were explained in present research [30]. The correlation algorithm to process the PIV raw images was used Fast Fourier Transform (FFT) to reduce the computational cost. The PIV image time interval was selected as 20 μs during intake strokes because the velocity of in-cylinder flow was relatively high compared to the compression strokes during which time interval was 40 μs. The specifications of the PIV system are given in Table 2.

4. Computational details

4.1. Simulation model description

To simulate the two-cylinder high compression ratio GDI engine, CONVERGE v2.4 was used. The RNG k-ε model [31,32] was used as a turbulent model to close the RANS equation. For modeling high-pressure gasoline injection of about 700 bar, the KH-RT model was used.

4.2. Simulation condition

The computational domain in Fig. 2 consists of the intake manifold, exhaust manifold, cylinder 1, and cylinder 2 (the data for analysis was calculated from cylinder 1). The SCV was located in one of the intake ports of each cylinder. The SCV angles of 0°, 30°, 45°, 60°, 90° were considered to investigate the in-cylinder flow characteristics for those angles. At the 90° SCV angle, the SCV was flipped into the opposite direction to the other conditions.

The injection system included a center-mount, spray-guided injector which injected the fuel at high pressure for enhanced atomization. And the spark plug was located between the exhaust valves. To simulate the gasoline spray break-up process, isooctane was used as a gasoline surrogate fuel. The detailed simulation conditions described in Table 3. Boundary conditions were set at the inlet and outlet of the intake and exhaust manifolds based on the PIV experiment conditions. The simulation was started at the intake valve opening, so that the initial in-cylinder condition was set to be the same as the intake condition, and to reduce the errors from the initial conditions, the results of the second cycle were used. Based on simulation results for the base grid sizes of 3.5, 4.0, 5.0, and 6.0 mm to select the base grid size (Table 4), the simulation was conducted at 4.0 mm in consideration of the simulation time and accuracy. In addition, it was set to 1/2 the size of the base grid through grid embedding on the inside of the cylinder. Adaptive mesh refinement was also performed based on the velocity difference of 2.5 m/s.

Table 1
Engine specifications.

Compression ratio	14
Bore	75.6 mm
Stroke	83.38 mm
Conrod length	147.8 mm
Displacement (two-cylinder)	748.5 cc
Rated RPM	6300 rpm
IVO	bTDC 332 deg
IVC	bTDC 114 deg
EVO	aTDC 152 deg
EVC	aTDC 370 deg

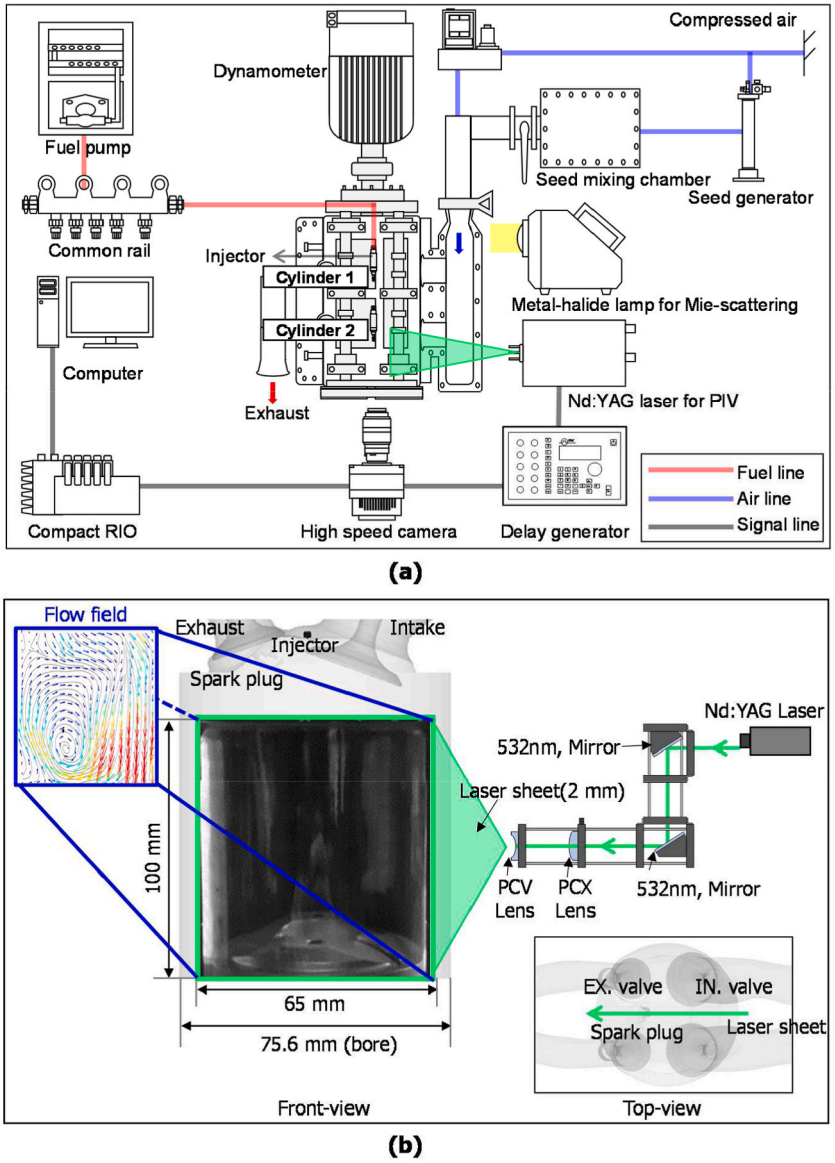

Fig. 1. Schematic diagrams of an experiment setup: (a) optically accessible engine system, and (b) PIV optical system.

Table 2
Specifications of the PIV system.

Items	Details
Camera	High speed camera (Phantom, VEO 710 L)
Laser	Nd:YAG pulse laser (26 mJ, double cavity)
Region of interest	65 × 100 mm
Resolution	320 × 344 pixels
Seed	10 μm, hollow sphere glass
PIV image time interval (dt)	Intake stroke: 20 μs Compression stroke: 40 μs
Interrogation area	32 × 32 pixels (50% overlap)
Correlation algorithm	FFT (Fast Fourier Transform)

4.3. Data analysis

The tumble flow was imaged at the tumble plane which is the center of the cylinder. The swirl flow was imaged at swirl planes 1, 2, and 3, respectively located 1.24 cm, 3.24 cm, and 5.24 cm from head as shown in Fig. 3 (a). The swirl ratio and the tumble ratio were

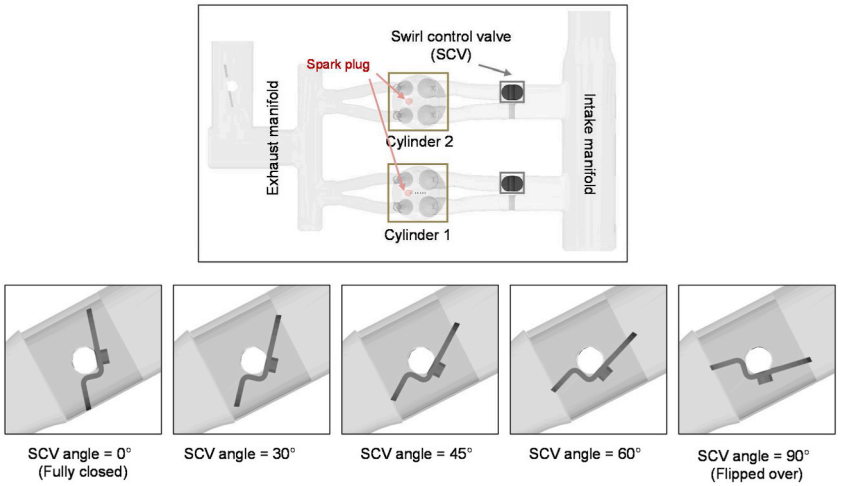

Fig. 2. Computational domain and the SCV angles.

Table 3
Simulation conditions.

Engine speed	1500 rpm	
Intake pressure	1.0 bar	
Intake temperature	308.15 K	
Outlet pressure	1.0 bar	
Outlet temperature	325 K	
Initial in-cylinder pressure	1.0 bar	
Initial in-cylinder temperature	308.15 K	
Piston temperature	480 K	
Liner temperature	450 K	
Head temperature	520 K	
SCV angles	In-cylinder flow simulation	0°, 30°, 45°, 60°, 90°
	Mixture formation simulation	0°, 45°
Injection type	Center-mount type	
Injection pressure	700 bar	
Injection quantity	23 mg	
Injection timing	bTDC 300 deg ~ bTDC 120 deg (30 deg interval)	

Table 4
Maximum in-cylinder pressure for different base grid size.

Base grid size	Maximum in-cylinder pressure
3.5 mm	1.144 MPa
4.0 mm	1.145 MPa
5.0 mm	1.138 MPa
6.0 mm	1.145 MPa

calculated as in Eqs. (1) and (2), where $\omega_{swirl\ plane}$ is the angular velocity of the flow about the center of the mass in the swirl direction, $\omega_{tumble\ plane}$ is the same but in the tumble direction, and $\omega_{crank\ shaft}$ is the angular velocity of the crank shaft.

$$Swirl\ ratio = \omega_{swirl\ plane} / \omega_{crank\ shaft} \tag{1}$$

$$Tumble\ ratio = \omega_{tumble\ plane} / \omega_{crank\ shaft} \tag{2}$$

To evaluate whether the flow characteristics for the different SCV angles were swirl-dominant or tumble-dominant, S/T, which is the ratio of maximum swirl intensity over time and the maximum tumble intensity over time, was used. S/T is calculated as shown in Eq. (3), where t defines the period from the intake valve opening to the top dead center (TDC).

$$S/T = Max(Swirl\ ratio(t))/Max(Tumble\ ratio(t)) \tag{3}$$

The spark plug gap was defined as the region within a radius of 1 mm from the center of the electrodes. The spark plug gap velocity was calculated and we considered the mass averaged velocity magnitude in the cell within the spark plug gap region which is described

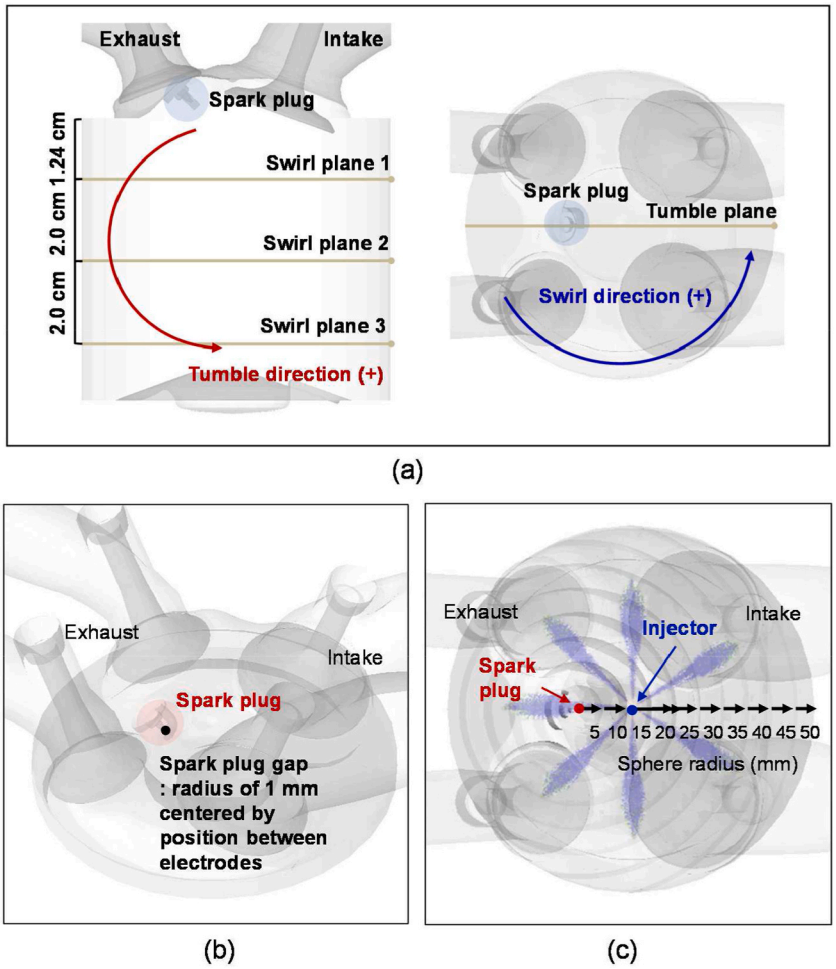

Fig. 3. Description of (a) analysis planes, (b) spark plug gap, and (c) location of spark plug and injector.

in Fig. 3 (b).

The mixture preparation can be assessed from the spatial distribution of the fuel. As shown in Fig. 3 (c), the spark plug and injector were located respectively between the exhaust valves, and in the center of cylinder, and the spray plumes included one plume targeting the spark plug. The equivalence ratio (ER) distribution from the spark plug can be used to evaluate the mixture properties, such as homogenous, stratified, or mal-distributed. As characterized by Addepalli, S.K. et al. [33], if the slope of the graph of the mean ER from the spark plug is 0, it is a homogeneous mixture. When the graph has a negative slope, it means that the fuel is concentrated near the spark plug, indicating a stratified mixture. The other shapes in the graph with a positive slope or a varying slope reveal non-effective fuel distribution for the combustion, which is here referred to as mal-distribution. The mean ER was calculated as the mass average ER in the cells within the interval of 5 mm from the spark plug, as demonstrated in Eq. (4):

$$Mean\ ER = \sum_{i=x}^{x+5} (mass \times ER) \Big/ \sum_{i=x}^{x+5} mass \tag{4}$$

where x is the distance from the spark plug, in mm.

4.4. Model validation

To secure the accuracy of the simulation results, model validation was conducted based on the PIV experiment results for the flow fields and the Mie scattering experiment results for the spray structures.

Comparison of the flow characteristics between the PIV experiments and the simulations was carried out for SCV angles 0°, 45°, and 90° at an engine speed of 1500 rpm and intake pressure of 1.0 bar. The velocity distribution at the tumble plane was compared in Fig. 4 (a)-(c). It can be seen that the simulation results reflected well the PIV experiment results in terms of flow field over time and variation of SCV angles. Additionally, for the quantitative comparison, the tumble ratio was used as a representative value of the flow in the tumble plane. As shown in Fig. 4 (d)–(f), the simulation results of the tumble ratio well matched the PIV experiment results, except at

bTDC 270 deg for SCV angles 45° and 90°. At bTDC 270 deg, the intake velocity was fast as shown in flow field comparison results, and imaging area of the PIV experiment was small. Furthermore, the pent-roof region which has a high velocity distribution during initial intake process and contributes greatly to the tumble ratio, was not reflected for the calculation of the tumble ratio in PIV experiment. However, when considering the flow and the overall tumble development, the accuracy of the simulation was confirmed.

In the previous study [30], the spray breakup model was validated based on experiment in constant volume chamber. This validated model had a good agreement in injection pressure of 700 bar in spray-guided gasoline direct injection. Therefore, it was used in this study for mixture formation simulation.

5. Results and discussion

5.1. Air flow characteristics for various SCV angles

5.1.1. Flow in the intake port

As shown in Fig. 5 (a), the velocity from the intake port without an SCV and the intake port with an SCV varied at different SCV angles. At the SCV angle 0°, the flow velocity in the port with an SCV was intensified. With an SCV, the in-cylinder flow differences for various SCV angles were initially from the velocity differences in the intake port during the intake process. Thus, the velocity difference (V_d) between the ports is shown in Fig. 5 (b) and was calculated as in Eq. (5):

$$V_d = V_{port\ w/o\ SCV} - V_{port\ w/\ SCV} \tag{5}$$

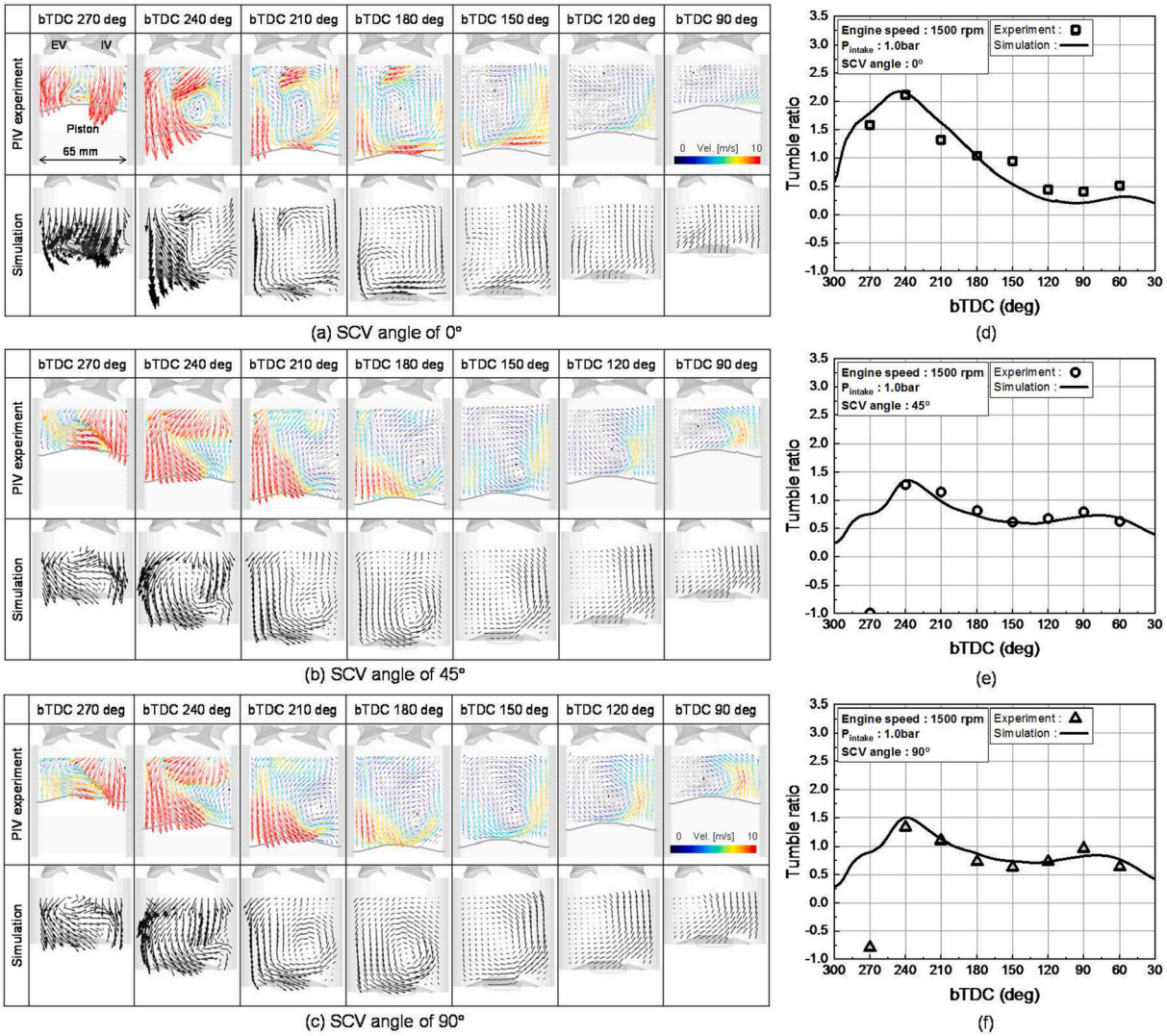

Fig. 4. Comparison between the PIV experiments and simulations of velocity distribution for (a) SCV angle 0°, (b) SCV angle 45°, and (c) SCV angle 90°, and tumble ratio for (d) SCV angle 0°, (e) SCV angle 45°, and (f) SCV angle 90°.

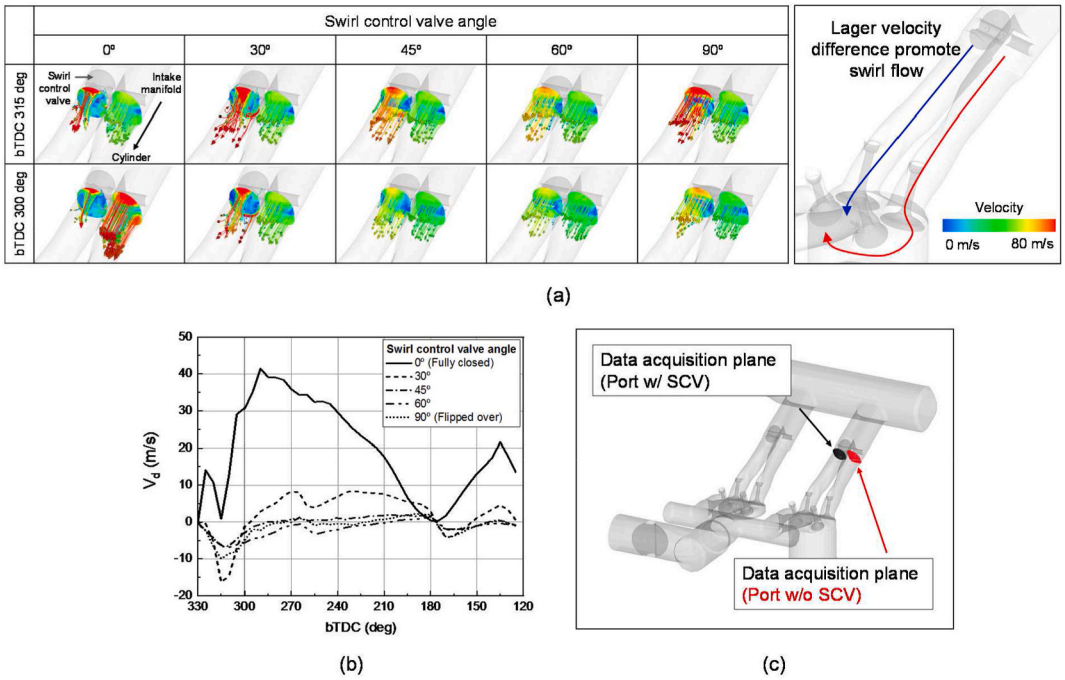

Fig. 5. (a) Intake flow velocity at the intake port lines for different SCV angles, (b) Velocity difference (V_d) between the port line without an SCV and port line with SCV at data acquisition planes in (c).

V_d decreased from the 0° to the 60° SCV angles because of the flow path open area in the port with an SCV. At the 90° SCV angle that is flipped over in Fig. 5 (c), the V_d had a value similar to the 45° SCV angle because the flow path area of the intake port with the 90° SCV angle was similar to that with an SCV angle of 45°.

5.1.2. In-cylinder flow development

To compare the swirl flow field for different SCV angles, the velocity distribution in the three swirl planes (in Fig. 6 (b)) was compared at bTDC 240 deg with the largest swirl ratio. As the V_d increased, the intake air velocity supplied from the intake port without an SCV became stronger, facilitating the swirl flow rotating along the liner wall. Thus, the velocity distribution in the swirl plane at the SCV 0° reveals an obvious clockwise swirl flow in Fig. 6 (a). In other conditions, strong rotation was not observed in the plane close to the intake valve (swirl plane 1) due to the interference of the flow supplied from each intake port, but in the plane close to the piston (swirl plane 3), such interference was weak, and the smaller the V_d, the weaker the rotation. The swirl flow can be quantitatively represented by the swirl ratio. The swirl ratio decreased as the SCV angle increased from 0° to 60°, and the same as the trend of V_d, the swirl ratio at 90° had a similar value to the swirl ratio at 45° as shown in Fig. 6 (c). The swirl flow was enhanced from intake valve opening to bTDC 240 deg, a period during which intake valve lift increased. After that, when the intake flow was weakened followed by the intake valve closing, the swirl ratio gradually decreased because no additional momentum was supplied in the swirl plane.

The in-cylinder tumble flow was affected by the intake valve lift and the piston movement. Thus, in this study, the four periods were defined during the intake and compression process based on the intake valve lift and piston speed, as shown in Fig. 7 (a). It shows different tumble flow characteristics in each defined period. The tumble flow development over time is shown in Fig. 7 (c). In period 1, the intake valve lift increased to the maximum lift and the piston rapidly moved downward. The intake flow could enter the cylinder smoothly through the intake valve without interfering with the inertia, and a high-velocity field could be formed in the cylinder as well by the piston's rapid downward movement. In period 2 the intake valve lift decreased and the piston downward speed decreased to under 5 m/s. In this period, the flow direction from the intake port and the intake valve movement direction were opposite, so the intake flow was disturbed and weakened and the relatively slow piston downward movement resulted in the weaker in-cylinder flow than in period 1. In period 3, the piston began to move upward, reinforcing the in-cylinder flow upward speed on the right side of the cylinder. period 4 is from the intake valve closing to the TDC. In period 4 the in-cylinder flow weakened when the intake valves were closed, with a reduced radial area for tumble rotation by the compression process.

The tumble ratio reflects the in-cylinder turbulent flow characteristic for the four periods in Fig. 7 (b). At the SCV angle 0°, the total intake port area was decreased so that the intake velocity during period 1 was the fastest. This resulted in the highest tumble ratio peak occurring in period 1 compared to the other SCV angle conditions. When the compression process started, the tumble ratio rose due to the effect of the piston movement through period 3, but at the 0° SCV angle the momentum was concentrated in the swirl flow, so that the tumble increase in period 3 was reduced compared to the other conditions. In the tumble flow, unlike the swirl flow, the radial area for rotation was reduced during the compression process. Therefore, the tumble ratio was reduced to less than 0.5 in all conditions near

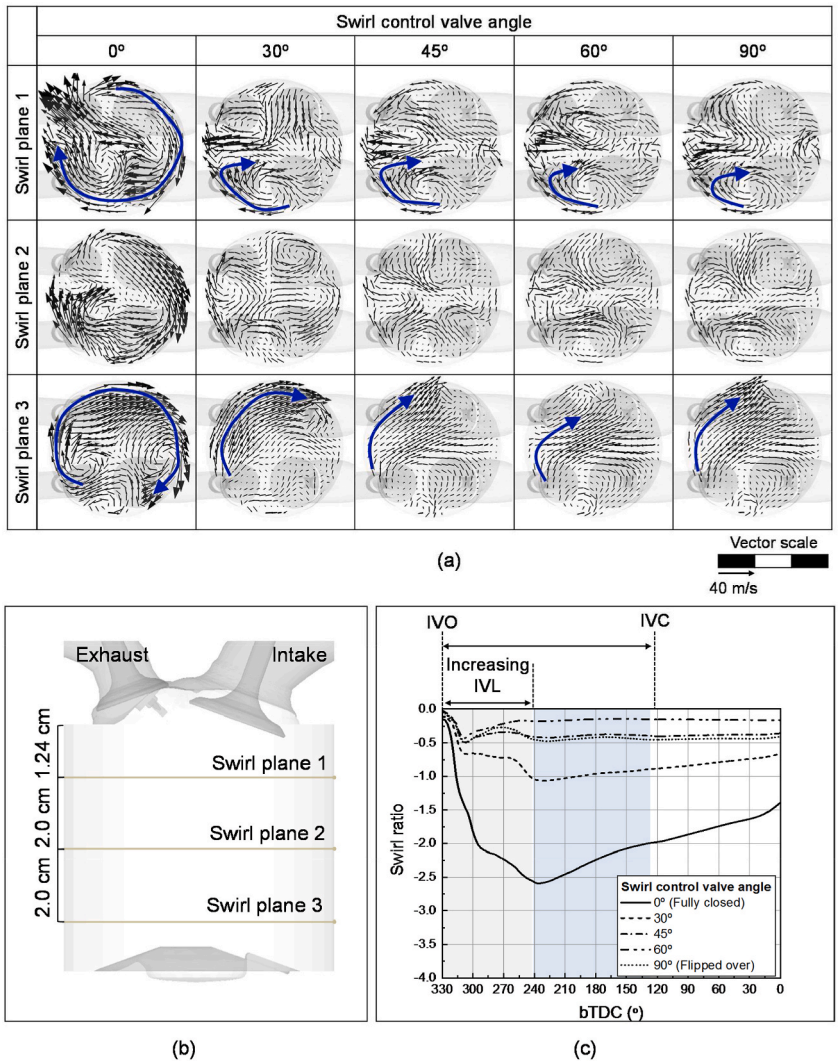

Fig. 6. (a) Swirl flows at bTDC 240 deg at swirl planes in (b), (c) Swirl ratio for different SCV angles.

the TDC.

With the SCV angles decreasing from 45° to 0°, the maximum swirl and tumble were intensified as shown in Table 5 of the maximum tumble ratio and swirl ratio. At the SCV angle higher than 45°, the effect of the SCV angle change was almost insignificant. The flow characteristics reflected whether it was swirl-dominant or tumble-dominant based on S/T; the swirl-dominant flow was exhibited at the SCV angle of 0° where S/T was greater than 1, and the tumble-dominant flow was exhibited at SCV angle of 45° where S/T was less than 1.

5.1.3. In-cylinder flow characteristics near the TDC

Differences in flow characteristics, such as in-cylinder swirl flow and tumble flow, caused differences in the spark plug gap flow near the TDC, which has an important role in spark stretching and early flame development. In the compression process, the difference of flow characteristics due to the SCV angle near the TDC was determined by the swirl intensity because of the reduced radial area for tumble rotation. Therefore, the closer to the swirl-enhancing condition, the stronger the spark plug gap velocity near the TDC (Table 6) which was calculated based on spark plug gap region in Fig. 3(b).

5.2. Spray development

Since the flow intensity and characteristics in the cylinder differed depending on the crank angle and SCV angles, the effect of flow on the spray structure was investigated through the captured images for different injection timing at after start of injection 8 deg (Fig. 8). At the injection timing of period 1, more spray dispersion was observed at the SCV angle of 0° than at 45°. However, the effect of the SCV angle on the spray structure and penetration was not significant during injection in periods 2, 3, and 4. This was because the flow intensity was relatively weak in the corresponding periods, which was insufficient to affect the high-pressure spray at 700 bar. The

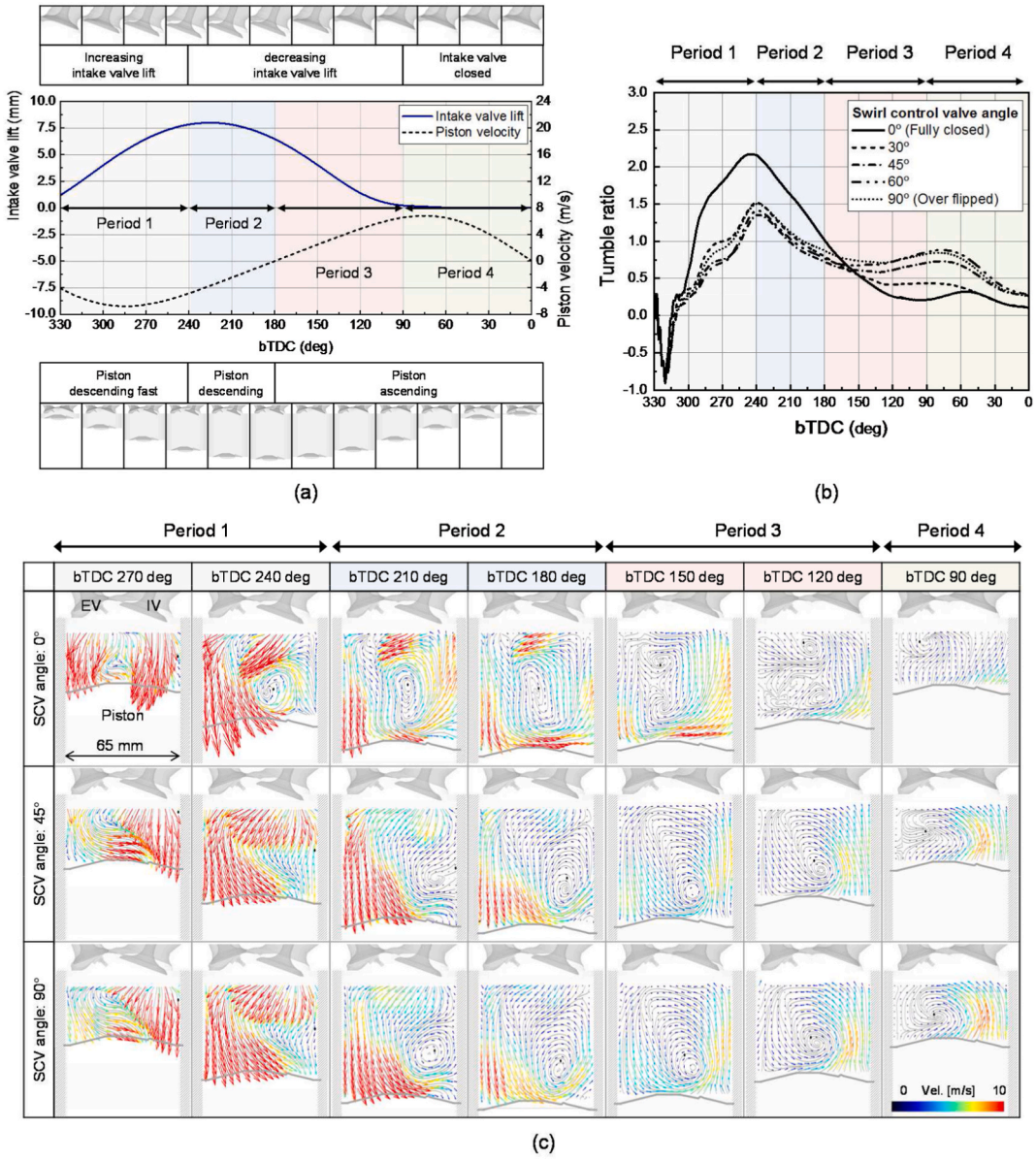

Fig. 7. (a) Period separation based on the intake valve lift and piston velocity, (b) tumble ratio and (c) tumble distribution for different SCV angles.

Table 5
Quantitative flow characteristic for different SCV angles.

Swirl control valve angle	Max. tumble ratio value	Max. swirl ratio value	S/T
0°	2.17	2.59	1.19
30°	1.52	1.01	0.70
45°	1.35	0.49	0.36
60°	1.42	0.43	0.30
90°	1.50	0.50	0.33

only observed changes in the spray structure depended on the change in the pressure inside the cylinder. During the compression process through periods 2, 3, and 4, the pressure inside the cylinder rises, and the spray plumes became thinner under the influence of the atmospheric pressure in both of SCV angle 0° and 45°. However, the mixing process of evaporated fuel which has been lost momentum by injection pressure is affected by the flow field and injection timing. Therefore, the mixing characteristics of the swirl dominant and tumble dominant flow were investigated through simulation.

Table 6
Spark plug gap velocity for different SCV angles at bTDC 15 deg.

Swirl control valve angle	Spark plug gap velocity magnitude
0°	6.69 m/s
30°	4.40 m/s
45°	1.89 m/s
60°	2.51 m/s
90°	2.03 m/s

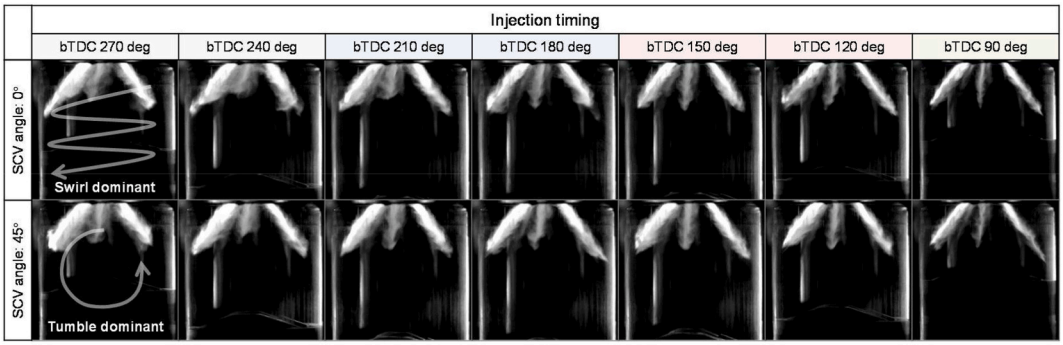

Fig. 8. Spray structure at after start of injection 8 deg for different injection timings.

5.3. *Mixture characteristics*

To evaluate the mixture characteristics, the spatial fuel distribution was calculated with different injection timing at SCV angles of 0° (swirl-dominant) and 45° (tumble-dominant).

In Fig. 9, the spatial fuel distribution is shown at the SCV angle of 0° for different injection timings. With retarded injection timing, the mixture characteristics were either homogeneous, mal-distributed, or stratified. As can be seen from the mixture formation process, in the case of a mal-distribution, the rich area formed in the intake valve side. It was also confirmed that the characteristics of the mixture for different injection timings were classified based on the characteristic time period divided by the relationship between the intake valve lift and the piston velocity, as discussed in Section 5.1.2.

In the case of SCV angle 45°, where the tumble was dominant from the intake to the compression processes, the retarded injection timing produced mixtures that were either homogeneous, stratified, or mal-distributed, as shown in Fig. 10. When the injection timing was in period 3, the mal-distributed mixture appeared in the form of creating a rich area between the intake and exhaust valves because there was not enough time to move toward the spark plug by tumble flow. As with the SCV angle of 0°, the time period that can distinguish the characteristics of the mixture could be divided based on the relationship between the intake valve lift and the piston velocity.

6. Conclusion

In this study, the influence of the SCV angle on the flow enhancement and mixing process in an high compression ratio spray-guided GDI engine was investigated using PIV experiments and CFD simulations. The main conclusions are as follows.

(1) When the SCV angle was less than 45°, the smaller the angle, the greater the difference in the flow rate supplied from the ports and the stronger the swirl. The swirl flow was enhanced from the intake valve opening to bTDC 240 deg, at which the intake valve lift increased.
(2) The tumble flow characteristics were determined by the intake valve lift and piston velocity. Accordingly, the tumble development process could be divided into four periods. At the SCV angle of 0°, which was a swirl reinforcement condition, the initially rapid intake flow was formed due to a decrease in the flow supply area at the intake port, so that the tumble was stronger in periods 1 and 2. However, after that the momentum was concentrated on the swirl flow and the tumble was rapidly weakened. Furthermore, the radial area for the tumble rotation was reduced during compression so that the tumble flow was weakened to a tumble ratio of 0.5 or less near the TDC under all SCV conditions. Therefore, the spark plug gap flow near the TDC was greatly affected by the swirl, and the spark plug gap velocity increased as the SCV angle decreased to 45° or less.
(3) Swirl-dominant flow and tumble-dominant flow could be differentiated by the ratio of the maximum swirl ratio and tumble ratio (S/T). It was judged that a swirl-dominant flow was formed at the SCV angle of 0° with an S/T of 1.19, and a tumble-dominant flow was formed at the SCV angle of 45° with an S/T of 0.36.
(4) In the injection timing, including period 1 where the intake flow was strong, the spray tended to fluster more under the swirl-dominant condition. However, in the subsequent injection timing, there were no apparent changes in the spray structures at various SCV angles.

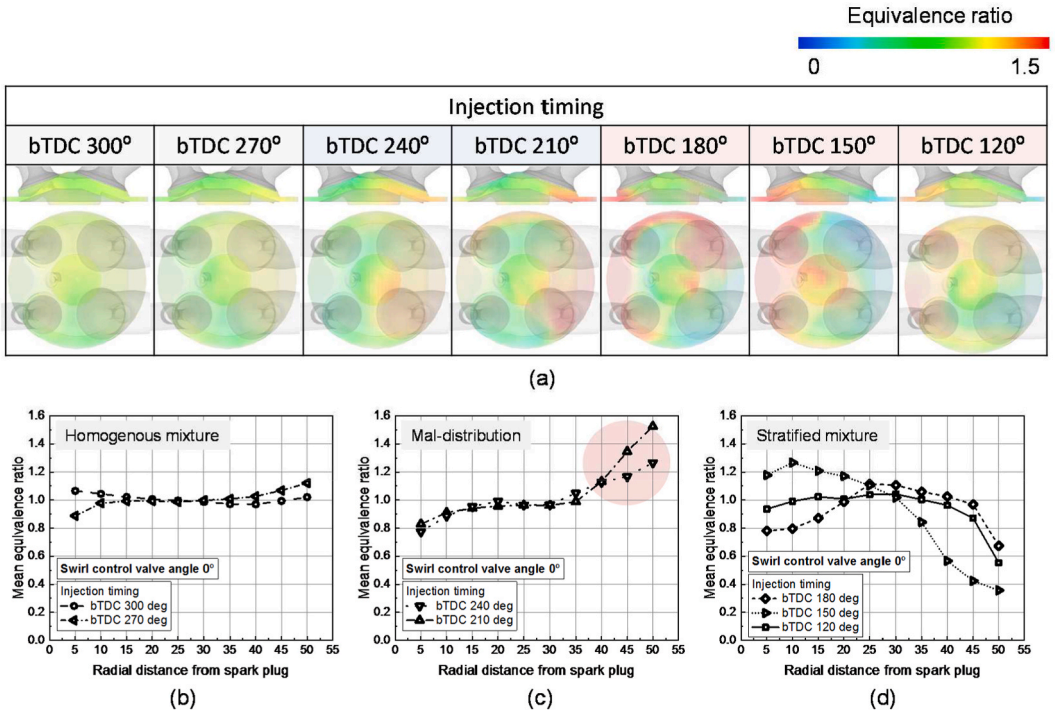

Fig. 9. (a) ER distribution and mean ER for the distance from the spark plug in the case of (b) injection in period 1, (c) injection in period 2 and (d) injection in period 3 at bTDC 10 deg for the SCV angle 0°.

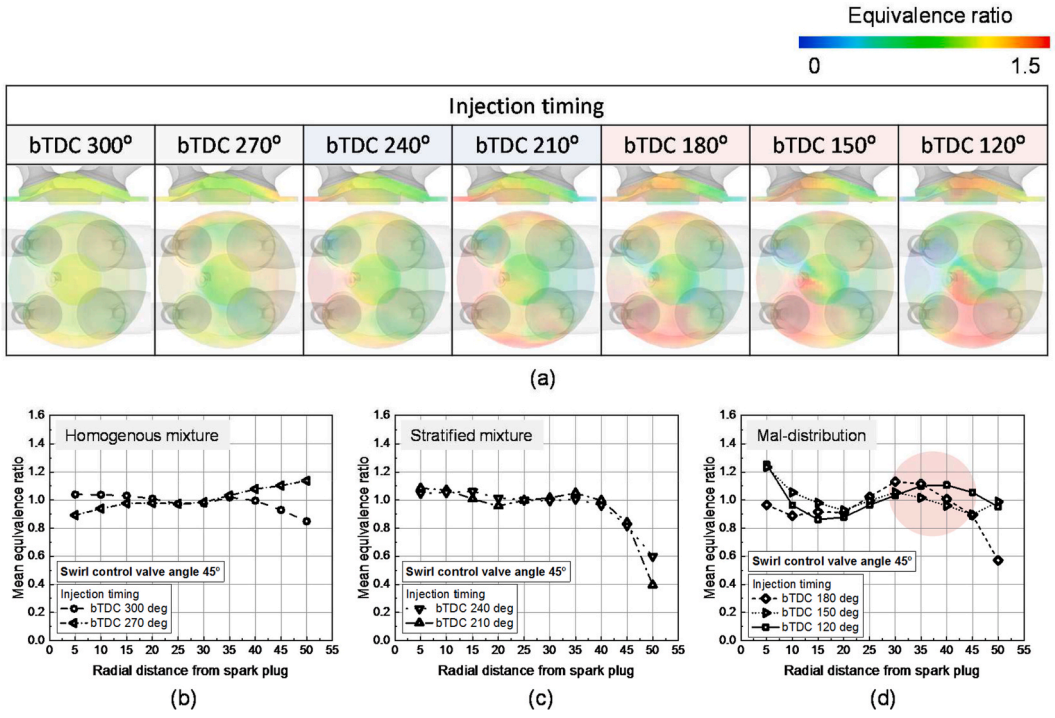

Fig. 10. (a) ER distribution and mean ER for the distance from spark plug in the case of (b) injection in period 1, (c) injection in period 2 and (d) injection in period 3 at bTDC 10 deg for the SCV angle 45°.

(5) In the mixing process of the evaporated fuel, the flow characteristics played an important role in determining the mixture characteristics. As a result, in the swirl-dominant flow, as the injection timing was more and more retarded, the mixture characteristics evolved in the order of homogeneous to mal-distributed to stratified. On the other hand, in the tumble-dominant flow, the mixture characteristics were in the order of homogeneous to stratified to mal-distributed as the injection timing was retarded. These characteristic time periods were classified based on the behavior of the intake valve lift and piston velocity.

CRediT authorship contribution statement

Jisoo Shin: Writing – original draft, Conceptualization, Methodology, Investigation, Experiments. **Donghwan Kim:** Writing – original draft, Investigation, Experiments. **Yousang Son:** Conceptualization, Methodology. **Sungwook Park:** Writing – review & editing, Supervision.

Declaration of competing interest

The authors declare that they have no known competing financial interests or personal relationships that could have appeared to influence the work reported in this paper.

Acknowledgements

This work was supported by Hyundai Motor Company and the National Research Foundation of Korea(NRF) grant funded by the Korea government (MSIT). (2021R1A2C2011425).

References

[1] T. Johnson, A. Joshi, Review of vehicle engine efficiency and emissions, SAE International Journal of Engines 11 (2018) 1307–1330, https://doi.org/10.2307/26649163.
[2] J.Y. Yong, V.K. Ramachandaramurthy, K.M. Tan, N. Mithulananthan, A review on the state-of-the-art technologies of electric vehicle, its impacts and prospects, Renew. Sustain. Energy Rev. 49 (2015) 365–385, https://doi.org/10.1016/j.rser.2015.04.130.
[3] Y. Balali, S. Stegen, Review of energy storage systems for vehicles based on technology, environmental impacts, and costs, Renew. Sustain. Energy Rev. 135 (2021) 110185, https://doi.org/10.1016/j.rser.2020.110185.
[4] C. Beatrice, C. Bertoli, M. Migliaccio, Basic concepts of the homogeneous charge compression ignition engines, ATA-TORINO- 55 (2002) 226–237.
[5] Y. Sun, W. Sun, L. Guo, H. Zhang, Y. Yan, W. Zeng, S. Lin, An experimental investigation of wide distillation fuel based on CTL on the combustion performance and emission characteristics from a CI engine, Fuel 310 (2022) 122262, https://doi.org/10.1016/j.fuel.2021.122262.
[6] F. Hadia, S. Wadhah, H. Ammar, O. Ahmed, Investigation of combined effects of compression ratio and steam injection on performance, combustion and emissions characteristics of HCCI engine, Case Stud. Therm. Eng. 10 (2017) 262–271.
[7] M.K. Mohammed, H.H. Balla, Z.M.H. Al-Dulaimi, Z.S. Kareem, M.S. Al-Zuhairy, Effect of ethanol-gasoline blends on SI engine performance and emissions, Case Stud. Therm. Eng. 25 (2021) 100891, https://doi.org/10.1016/j.csite.2021.100891.
[8] M. Mofijur, M.M. Hasan, T.M.I. Mahlia, S.M.A. Rahman, A.S. Silitonga, H.C. Ong, Performance and emission parameters of homogeneous charge compression ignition (HCCI) engine: a review, Energies (2019) 12, https://doi.org/10.3390/en12183557.
[9] B.-Q. He, S.-P. Xu, X.-Q. Fu, H. Zhao, Combustion and emission characteristics of an ultra-lean burn gasoline engine with dimethyl ether auto-ignition, Energy 209 (2020) 118437.
[10] M. Izadi Najafabadi, N. Abdul Aziz, Homogeneous charge compression ignition combustion: challenges and proposed solutions, Journal of combustion (2013) 2013, https://doi.org/10.1155/2013/783789.
[11] A. Vandersickel, M. Hartmann, K. Vogel, Y.M. Wright, M. Fikri, R. Starke, C. Schulz, K. Boulouchos, The autoignition of practical fuels at HCCI conditions: high-pressure shock tube experiments and phenomenological modeling, Fuel 93 (2012) 492–501, https://doi.org/10.1016/j.fuel.2011.10.062.
[12] W. Zhong, T. Pachiannan, Z. Li, Y. Qian, Y. Zhang, Q. Wang, Z. He, X. Lu, Combustion and emission characteristics of gasoline/hydrogenated catalytic biodiesel blends in gasoline compression ignition engines under different loads of double injection strategies, Appl. Energy 251 (2019) 113296, https://doi.org/10.1016/j.apenergy.2019.114018.
[13] J. Hunicz, M. Mikulski, Investigation of the thermal effects of fuel injection into retained residuals in HCCI engine, Appl. Energy 228 (2018) 1966–1984, https://doi.org/10.1016/j.apenergy.2019.114018.
[14] J. Hunicz, M. Mikulski, M.S. Geca, A. Rybak, An applicable approach to mitigate pressure rise rate in an HCCI engine with negative valve overlap, Appl. Energy 257 (2020) 114018, https://doi.org/10.1016/j.apenergy.2019.114018.
[15] J. Hunicz, Cycle-by-cycle variations in autonomous and spark assisted homogeneous charge compression ignition combustion of stoichiometric air–fuel mixture, Int. J. Spray Combust. Dyn. 10 (2018) 231–243, https://doi.org/10.1177/1756827718763564.
[16] Z. Wang, J. Wang, S. Shuai, X. He, F. Xu, D. Yang, X. Ma, in: Research on Spark Induced Compression Ignition (SICI), SAE Technical Paper, 2009.
[17] Z. Lee, T. Kim, S. Park, S. Park, Review on spray, combustion, and emission characteristics of recent developed direct-injection spark ignition (DISI) engine system with multi-hole type injector, Fuel 259 (2020) 116209, https://doi.org/10.1016/j.fuel.2019.116209.
[18] Mazda corporation: skyactiv technology. http://www.mazda.com/en/innovation/technology/skyactiv/. (Accessed 5 December 2021).
[19] S. Itabashi, E. Murase, H. Tanaka, M. Yamaguchi, T. Muraguchi, in: New Combustion and Powertrain Control Technologies for Fun-To-Drive Dynamic Performance and Better Fuel Economy, SAE Technical Paper, 2017.
[20] W. Zeng, M. Sjöberg, D.L. Reuss, PIV examination of spray-enhanced swirl flow for combustion stabilization in a spray-guided stratified-charge direct-injection spark-ignition engine, Int. J. Engine Res. 16 (2015) 306–322, https://doi.org/10.1177/1468087414564605.
[21] K. Lee, C. Bae, K. Kang, The effects of tumble and swirl flows on flame propagation in a four-valve SI engine, Appl. Therm. Eng. 27 (2007) 2122–2130, https://doi.org/10.1016/j.applthermaleng.2006.11.011.
[22] J. Yang, X. Dong, Q. Wu, M. Xu, Effects of enhanced tumble ratios on the in-cylinder performance of a gasoline direct injection optical engine, Appl. Energy 236 (2019) 137–146, https://doi.org/10.1016/j.apenergy.2018.11.059.
[23] S. Sayama, M. Kinoshita, Y. Mandokoro, T. Fuyuto, Spark ignition and early flame development of lean mixtures under high-velocity flow conditions: an experimental study, Int. J. Engine Res. 20 (2019) 236–246, https://doi.org/10.1177/1468087417748517.
[24] B. Johansson, Influence of the velocity near the spark plug on early flame development, in: SAE International Congress and Exposition, Society of Automotive Engineers, 1993.
[25] L. Chen, H. Wei, J. Pan, C. Liu, G. Shu, Understanding the correlation between auto-ignition, heat release and knocking characteristics through optical engines with high compression ratio, Fuel 261 (2020) 116405, https://doi.org/10.1016/j.fuel.2019.116405.
[26] L. Chen, H. Wei, C. Chen, D. Feng, L. Zhou, J. Pan, Numerical investigations on the effects of turbulence intensity on knocking combustion in a downsized gasoline engine, Energy 166 (2019) 318–325, https://doi.org/10.1016/j.energy.2018.10.058.

[27] X. Dong, J. Yang, Q.N. Chan, Influence of flash boiling and swirl ratio on the gasoline spray structure in a spark-ignition optical engine: an experimental study, J. Energy Inst. 94 (2021) 233–241, https://doi.org/10.1016/j.joei.2020.09.007.
[28] A.A. Hosseini, M. Ghodrat, M. Moghiman, S.H. Pourhoseini, Numerical study of inlet air swirl intensity effect of a Methane-Air Diffusion Flame on its combustion characteristics, Case Stud. Therm. Eng. 18 (2020) 100610, https://doi.org/10.1016/j.csite.2020.100610.
[29] W. Thielicke, E. Stamhuis, PIVlab–towards user-friendly, affordable and accurate digital particle image velocimetry in MATLAB, J. Open Res. Software (2014) 2.
[30] D. Kim, J. Shin, Y. Son, S. Park, Characteristics of in-cylinder flow and mixture formation in a high-pressure spray-guided gasoline direct-injection optically accessible engine using PIV measurements and CFD, Energy Convers. Manag. 248 (2021) 114819.
[31] V. Yakhot, S.A. Orszag, Renormalization group analysis of turbulence. I. Basic theory, J. Sci. Comput. 1 (1986) 3–51.
[32] V. Yakhot, S. Orszag, S. Thangam, T. Gatski, C. Speziale, Development of turbulence models for shear flows by a double expansion technique, Phys. Fluid. Fluid Dynam. 4 (1992) 1510–1520.
[33] S.K. Addepalli, O.P. Saw, J. Mallikarjuna, Effect of mixture distribution on combustion and emission characteristics in a GDI engine-A CFD analysis, in: SAE Technical Paper, 2017.